

Adversarial Attacks with Time-Scale Representations

Alberto Santamaria-Pang, Jianwei Qiu, Aritra Chowdhury, James Kubricht,
Peter Tu, Iyer Naresh, Nurali Virani
GE Research, 1 Research Circle, Niskayuna, NY 12309

{santamar, jianwei.qiu, Aritra.Chowdhury, james.kubrich, tu, iyerna, nurali.virani}@ge.com

Abstract

We propose a novel framework for real-time black-box universal attacks which disrupts activations of early convolutional layers in deep learning models. Our hypothesis is that perturbations produced in the wavelet space disrupt early convolutional layers more effectively than perturbations performed in the time domain. The main challenge in adversarial attacks is to preserve low frequency image content while minimally changing the most meaningful high frequency content. To address this, we formulate an optimization problem using time-scale (wavelet) representations as a dual space in three steps. First, we project original images into orthonormal sub-spaces for low and high scales via wavelet coefficients. Second, we perturb wavelet coefficients for high scale projection using a generator network. Third, we generate new adversarial images by projecting back the original coefficients from the low scale and the perturbed coefficients from the high scale sub-space. We provide a theoretical framework that guarantees a dual mapping from time and time-scale domain representations. We compare our results with state-of-the-art black-box attacks from generative-based and gradient-based models. We also verify efficacy against multiple defense methods such as JPEG compression, Guided Denoiser and Comdefend. Our results show that wavelet-based perturbations consistently outperform time-based attacks thus providing new insights into vulnerabilities of deep learning models and could potentially lead to robust architectures or new defense and attack mechanisms by leveraging time-scale representations.

1. Introduction

While great progress has been made in adversarial attacks [3, 6, 16, 41], the fundamental reason why convolutional neural networks (CNNs) are fragile to small perturbations is still unclear [25, 33, 4, 44, 32]. State-of-the-art models generate perturbations that seem like statistical noise that affect both high and low image scales (similar to high

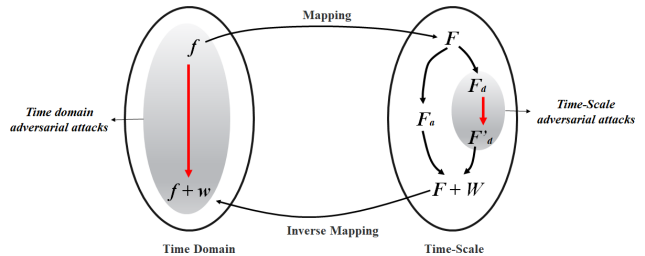


Figure 1. Schematic of the proposed Time-Scale adversarial attack.

and low frequency). We believe that the inability to localize an attack becomes a key limitation of time-domain attacks as they end up modifying unnecessary or unrelated information in the image [20, 2]. Thus, instead of generating adversarial attacks in the time domain (low and high frequencies), we propose to expose a new vulnerability of deep learning models by generating fine structural-perturbations in meaningful image content in the high scale Wavelet decomposition. Studies have shown that early convolution layers capture low-level edge and edge orientation information possibly similar to receptive fields of human vision [19, 49]. We aim to induce a perturbation that will alter the local vertical, horizontal, and diagonal edge content of images, therefore, creating arbitrary activation spikes in early convolution layers. We argue that decomposing and isolating localized coherent spatial arrangements is an effective mechanism for disrupting CNN layer responses. Our approach relies on the following steps: i) time-scale analysis is used to provide a mechanism to decompose an image and localize high scale (frequency) and structural image properties, ii) generative models are used to learn both high-scale and structural patterns to perturb high scale coefficients, iii) synthesis of image from perturbed coefficients aims disrupt early convolution layers. Figure 1 presents a schematic of our proposed method.

Since, state-of-the-art deep learning (DL) network designs rely on convolutional layers that broadly target all high frequency content – indiscriminate to structural per-

turbations – making them highly vulnerable to these attacks [34, 1, 42, 48, 5]. The targeted decomposition of fine image details accounts for a small fraction of the image energy content [24, 14, 8]. This helps with our objective to minimally perturb the image while inducing misclassification in classifier that consist of convolution layers. The significance of our approach is that the concept of scales (wavelet decomposition levels) and orientations (filter banks) can be associated to one another to investigate the fundamental principles of image/video analysis and signal processing for a new type of black-box attack.

2. Literature Review

To the best of our knowledge, no work has been reported in attack-based mechanisms from time-scale representations. All adversarial attack frameworks reported to date [30, 21, 37, 27, 10, 7, 6, 40, 45, 18, 43], perturb an image which is represented in the time domain using all of its frequency (Fourier) content. A detail review can be found in Pitropakis *et al.* [28]. Black-box attacks are challenging adversarial attacks as there is no access to training data nor to the target model. These attacks can be categorized as either *gradient-based* or *transfer-based* methods. *Gradient-based* methods iteratively estimate the gradient by perturbing the input image while optimizing an objective function. Here the major challenge is to account for robust optimization in a high dimensional input space (see Chen *et al.* [6] for an initial report). Ilyas *et al.* [16] subsequently proposed a natural evolution attack with a limited number of queries. While their methods showed a significant improvement in query efficiency and speed, it generated images with high distortion. Performance was later improved by Cheng *et al.* [7] who used a surrogate model as a prior, effectively reducing the number of gradient averages or queries per iteration.

To alleviate computational cost, *transfer-based* attacks [29, 35, 36, 12] train a generator network using white-box attacks from a surrogate or a chosen base model. Sharif *et al.* [35] used adversarial generative networks to create adversarial examples with defined objectives. The method was demonstrated in applications for face and handwritten-digit recognition. Poursaeed *et al.* [29] presented an approach that uses a generative model to design small perturbations (high frequency) that are distributed in the overall image, rather than following structural patterns. All of the above methods share the following limitations: *gradient-based* methods are prohibitively computationally expensive when estimating the gradient, while *transfer-based* methods suffer from generalization. *Our hypothesis* is that accounting for unnecessary and redundant image content in very high multidimensional space leads to non-tractable optimization problems and poor generalization [9, 42, 46, 26, 39].

Our main contributions are the following: i) providing a novel, tractable, fast, and black-box (surrogate-based or transfer-based) adversarial attack for deep neural networks, ii) exploring a new direction to study vulnerability (and hence robustness) of neural networks via time-scale perturbations that affects early convolution layers, and iii) experimental study with state-of-the-art classifiers and other generative or iterative attacks to illustrate the efficacy and salient features of this attack. Our code is available online at: <https://github.com/waveletgap/wgap>.

3. Methods

3.1. Background

Multiresolution Analysis: We briefly review multiresolution analysis introduced by Mallat and Meyer from [23]. Let φ a function in $L^2(\mathbb{R})$ (Hilbert space of square-integrable complex valued functions on \mathbb{R}), such that the translation $\varphi(\cdot - k), k \in \mathbb{Z}$ defines an orthonormal system. Then φ generates the sequence of spaces $V_j : j \in \mathbb{N}$, if $\varphi_{jk}(x) = 2^{j/2}\varphi(2^jx - k)$. A multiresolution analysis (MRA) for $L^2(\mathbb{R})$ is a sequence of spaces $\{V_j\}$ generated by the orthonormal system φ_{jk} in $L^2(\mathbb{R})$, if $V_j \subset V_{j+1}$ and $\bigcup V_j$ is dense in $L^2(\mathbb{R})$. We say that φ is a *father wavelet* or scaling function if φ generates a MRA. Given $f \in L^2(\mathbb{R})$, it can be shown that $f \in \bigcup_{j=0}^{\infty} V_j = V_0 \oplus \bigoplus_{j=0}^{\infty} W_j$, where W_j is the orthogonal complement of V_j in V_{j+1} . We refer to W_j as j^{th} resolution level of the multiresolution analysis of level j . A *mother wavelet* is a function $\psi \in W_0$ such that $\psi_{0k} = \psi(\cdot - k)$. Then ψ is an orthonormal basis in W_j and is orthogonal to the father wavelet. Then any $f \in L^2(\mathbb{R})$ can be represented in terms of the father and mother wavelet via the following series:

$$f(x) = \sum_k \alpha_k \varphi_{0k}(x) + \sum_{j=0}^{\infty} \sum_k \beta_{jk} \psi_{jk}(x), \quad (1)$$

where the wavelet coefficients are defined as: $\alpha_k = \int f(x) \overline{\varphi_{0k}(x)} dx$, $\beta_{jk} = \int f(x) \overline{\psi_{jk}(x)} dx$. The main advantage of the wavelet representation in Eq. 1 over Fourier analysis is the ability to capture both the *spatial component* and the *frequency spectrum*. The term $\sum_k \alpha_k \varphi_{0k}(x)$ is the *spatial component* whereas the term $\sum_{j=0}^{\infty} \sum_k \beta_{jk} \psi_{jk}(x)$ localizes the *frequency spectrum*. The coefficients α_k inherently capture the main signal content while β_{jk} capture the local details. We refer to α_k and β_{jk} as the approximation and detail coefficients, respectively.

2D Discrete Wavelet Transform (DWT): The 2D Discrete Wavelet Transform (DWT) is a direct generalization of the 1D MRA into $L^2(\mathbb{Z}^2)$. Let φ be a scaling function and ψ its corresponding wavelet. We define three wavelets: $\psi^1 = \varphi\psi$, $\psi^2 = \psi\varphi$, and $\psi^3 = \varphi\varphi$,

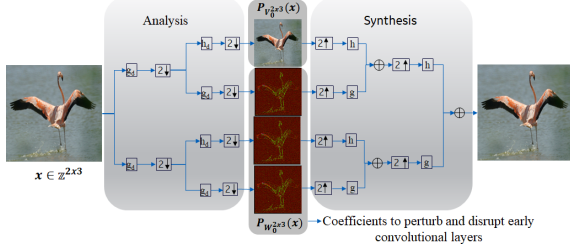


Figure 2. Schematic of the 2D wavelet transform for an RGB image x showing associated filter banks for analysis and synthesis. The input image is projected into $P_{V_0}^{2 \times 3}$ and $P_{W_0}^{2 \times 3}$.

where $\psi_{j,(n_1,n_2)}^k(t_1, t_2) = 2^{j/2} \psi^k((2^j n_1 - t_1)/2^j, (2^j n_2 - t_2)/2^j)$ with $k \in \{1, 2, 3\}$. Then the wavelet family $\{\psi_{j,n}^1, \psi_{j,n}^2, \psi_{j,n}^3\}_{n \in \mathbb{Z}^2}$ with $n = (n_1, n_2)$ is an orthonormal basis for W_j^2 and $\{\psi_{j,n}^1, \psi_{j,n}^2, \psi_{j,n}^3\}_{j,n \in \mathbb{Z}^2}$ is an orthonormal basis for $L^2(\mathbb{Z}^2)$. The corresponding coefficients are obtained from the inner products: $a_j[n] = \langle f, \varphi_{j,n}^2 \rangle$, $d_{jk}[n] = \langle f, \psi_{j,n}^k \rangle$, $\forall k \in \{1, 2, 3\}$. The approximation coefficients a_j are associated with low frequencies, whereas the detail coefficients d_{jk} are associated with high frequencies at horizontal, vertical, and diagonal orientations. The scaling function φ and the mother wavelet ψ can be represented as conjugate mirror filters banks $h[n]$ and $g[n]$. We denote as $h_d[n] = h[-n]$ and $g_d[n] = [-g]$ the mirror filters of $h[n]$ and $g[n]$, respectively. Figure 2 illustrates two-dimensional DWT for the first decomposition level.

3.2. Wavelet-based Generative Adversarial Perturbation (WGAP) Modeling

We present a generic framework for black-box and transfer attacks by perturbing the projection $P_{W_{j_0}}(x)$ (details) and preserving the projection $P_{V_{j_0}}(x)$ (approximation) for an image x . The analysis is shown for single channel images $L^2(\mathbb{Z}^2)$, but is easily generalized to three-channel color images. Since it has been observed that early convolution layers capture low-level edge and edge orientation information, we aim to induce a perturbation in $P_{W_{j_0}}(x)$ such that it will alter the local vertical, horizontal, and diagonal edge content of x , therefore, creating arbitrary activation spikes in early convolution layers. This method systematically alters the edges, thereby influencing shape-content information. This approach is different from denoising since noise distribution is not explicitly modeled. Rather, object structure from finer details is directly altered. We also deviate from intervention methods in the high-frequency Fourier spectrum since Fourier transformations lose spatial content coherence in contrast with time- and space-scale representations used in this work.

3.2.1 General Formulation

Suppose, we have a classifier $c(\cdot)$ with a loss function $\ell_c(X, y)$ where X and y is the input image and output class label, respectively. Here $c(X)$ is the predicted label. We assume: i) an adversarial example can be derived from an additive model as follows $X' = X + D$, and ii) for a fixed class label y , the loss ℓ_c is a continuous function. Then adversarial attack generation can be posed as an optimization problem:

$$\arg \max_{X': \|X' - X\| \leq \epsilon} \ell_c(X', c(X)). \quad (2)$$

Please note that: i) if $c(\cdot)$ is the attacked model then it is a white-box attack, ii) if it is a surrogate of the model to be attacked, then it is a black-box attack, and iii) if it is a chosen base model and the model to be attacked is unknown, then it is a transfer attack. Based on this formulation, in this work, we are interested in transfer and black-box attacks with perturbation in the wavelet domain. To convince that such an attack is sound, we look at the following result.

Theorem 1: Let (a_j, d_{jk}) , (a_j, d'_{jk}) be wavelet coefficients for X and X' , such that $X = \text{DWT}^{-1}(a_j, d_{jk})$ and $X' = \text{DWT}^{-1}(a_j, d'_{jk})$. For some scale j_0 , we can express problem in Equation 2 in terms of the wavelet coefficients as follows:

$$\arg \max_{\text{DWT}^{-1}(a_{j_0}, d'_{j_0 k}) : \|d_{j_0 k} - d'_{j_0 k}\| \leq \bar{\epsilon}} \ell_c(X', c(X)). \quad (3)$$

Proof. We need to prove that if $\|X' - X\| < \epsilon$, then there exists $\bar{\epsilon}$, such that $\|d_{j_0 k} - d'_{j_0 k}\| < \bar{\epsilon}$ for any chosen scale j_0 . Given that X and X' have the same approximation coefficients, from Equation 1, $D = X' - X$ is in $W_{j_0}^2$ but not in V_{j_0} . Then using, linearity, orthonormality and the Pythagorean identity, we can write $\|X - X'\|$ as:

$$\left\| \sum_{j=0}^{\infty} \sum_k d_{jk} \psi_{jk}(X) - \sum_{j=0}^{\infty} \sum_k d'_{jk} \psi_{jk}(X') \right\| = \quad (4)$$

$$\left\| \sum_{j=0}^{\infty} \sum_k (d_{jk} - d'_{jk}) \psi_{jk}(X - X') \right\| < \quad (5)$$

$$\sum_{j=0}^{\infty} \sum_k \|d_{jk} - d'_{jk}\| \|\psi_{jk}(X - X')\| \leq \quad (6)$$

$$\sup_{j,k} \|d_{jk} - d'_{jk}\| = \|d_{j_0 k} - d'_{j_0 k}\| = \bar{\epsilon} \quad (7)$$

Finally, the DWT is providing the dual mapping of the signal representation from the estimated detailed coefficients d' within $W_{j_0}^2$ respect to the loss function ℓ_c . \square

The intuition behind the previous formulation is that the dual space can create a new adversarial image by just perturbing the details coefficients corresponding to a scale level

(resolution) of the original image. The significance of this theoretical result is that i) adversarial attacks could be further targeted to an optimal resolution (scale and frequency) and ii) makes no assumption on the attack type since results applies to black-box, white-box and class-targeted attacks. Next, we will demonstrate a formulation for black-box and generative models.

3.2.2 Wavelet-based Generative Adversarial Perturbations

Poursaeed *et al.* [29] proposed a Generative Adversarial Perturbation (GAP) method to minimize cross entropy loss, targeting the least likely class for an input image and surrogate model c . Here, noise (from uniform distribution) is passed to a generator network to create a perturbation. Then, the output of the generator is normalized based on a maximum magnitude of perturbation and added to the original image to generate X' .

Time Domain Formulation: We formulate a novel universal loss function for universal black-box attacks: we do not use noise models and only use a surrogate model c . We propose a conditional loss function based on a budget parameter. This parameter controls the magnitude of the image perturbation. Comparing to normal cross entropy loss, the key difference is that we optimize the attack rate (fooling ratio) while keeping the amount of perturbation within certain budget ϵ . If perturbations exceeds the budget ϵ , an additional penalty term will be added to the total loss. The same concept can be applied to gradient-based methods and targeted attacks. For a given budget ϵ , the time domain representation of the loss function is:

$$\ell_c = \begin{cases} \mathcal{H}(p(X'), \mathbb{I}_{p_{lu}(X)}) + l * \mathcal{D}(X', X), & \text{if } \|X - X'\| > \epsilon \\ \mathcal{H}(p(X'), \mathbb{I}_{p_{lu}(X)}) & \text{otherwise} \end{cases} \quad (8)$$

The first term \mathcal{H} is the cross-entropy operator, where \mathbb{I}_y denotes the one-hot encoding for the class label y , probability $p(X')$ is output probability for perturbed sample, and $p_{lu}(X) = \arg \min p(X)$ is the least likely class given the original image X based on model c . For the second term, l is a parameter to regulate the loss, \mathcal{D} the structural dissimilarly:

$$\mathcal{D}(X', X) = 1 - \frac{(2\mu_{X'}\mu_X + c_1)(2\sigma_{X'X} + c_2)}{(\mu_{X'}^2 + \mu_X^2 + c_1)(\sigma_{X'}^2 + \sigma_X^2 + c_2)}, \quad (9)$$

where $\mu_{X'}$, $\sigma_{X'}$ represent the mean and covariance for X' (similarly for X), $\sigma_{X'X}$ is the covariance of X' and X . The values for c_1 , c_2 stabilize the division with weak denominator.

Dual Formulation: We reformulate the previous time-domain attack. From Theorem 1, given a budget ϵ , there is a scale j_0 so that $X = \text{DWT}^{-1}(a_{j_0}, d_{j_0k})$ and $X' =$

$\text{DWT}^{-1}(a_{j_0}, d'_{j_0k})$. The, the terms for Equation 8 from the following terms:

$$\mathcal{H}(p(\text{DWT}^{-1}(a_{j_0}, d'_{j_0k}), \mathbb{I}_{p_{lu}(\text{DWT}^{-1}(a_{j_0}, d_{j_0k}))}), \quad (10)$$

and

$$\mathcal{D}(\text{DWT}^{-1}(a_{j_0}, d'_{j_0k}), \text{DWT}^{-1}(a_{j_0}, d_{j_0k})), \quad (11)$$

where, $k \in \{1, 2, 3\}$. Similarly for the budget ϵ is estimated from DWT^{-1} . We show how we can use the notion of scale to constraint the magnitude of the perturbation (budget). In our implementation, we fixed a scale j_0 , and we apply DWT to obtain the approximation and detail coefficients a_{j_0} and d_{j_0k} . We only pass the detail coefficients d_{j_0k} to the generator and we reconstruct X' using inverse DWT from the original approximation coefficients a_{j_0} and the new perturbed coefficients d'_{j_0k} . Note that we are inherently normalizing the perturbed coefficients relative to the scale j_0 and this is possible because that approximation coefficients contain most of the energy. Figure 3 shows a schematic of the proposed method.

4. Results

We demonstrate model transferability of our Wavelet-based Generative Adversarial Perturbation (WGAP) method and compare performance with the generative model GAP [29] and a gradient-based method [7]. The ILSVRC12 (ImageNet-1000) dataset [31] was used for training, and 1000 randomly selected ImageNet images [7] were used for evaluation. The Generative model for GAP [29] and WGAP is a ResNet generator with 6 ResNet blocks, except the size of the input and output channels are different. The surrogate model is Inception-v3. To implement the discrete wavelet transform (DWT), we used the Daubechies wavelet filter bank db2 [8] at scale levels: 1, 2, 3 and budgets $\epsilon_1 = 0.05$, $\epsilon_2 = 0.1$, $\epsilon_3 = 0.25$. The selection of the Daubechies wavelet is due to stable numerical approximation and compact representation. For the WGAP models, nine input and output channels were used due to three concatenated detail coefficients. For the first convolution layer of the generative model, generative filter kernel size was set to 7 with a kernel number of 64. For the second and third convolution layers, the kernel size was 3 with a kernel number of 128. For each of the ResNet block, the kernel size as set to 3 a kernel number of 256. Batch normalization and ReLU activation function was used along with each convolution layer. The Adam optimization function was used with learning rate 0.0002 and beta parameters 0.5 and 0.999. The GAP and WGAP models were trained for 100 epochs with 500 iterations each. For GAP, we used magnitude value of 10. The models were then evaluated using a conventional NVIDIA V100-32G GPU and implemented

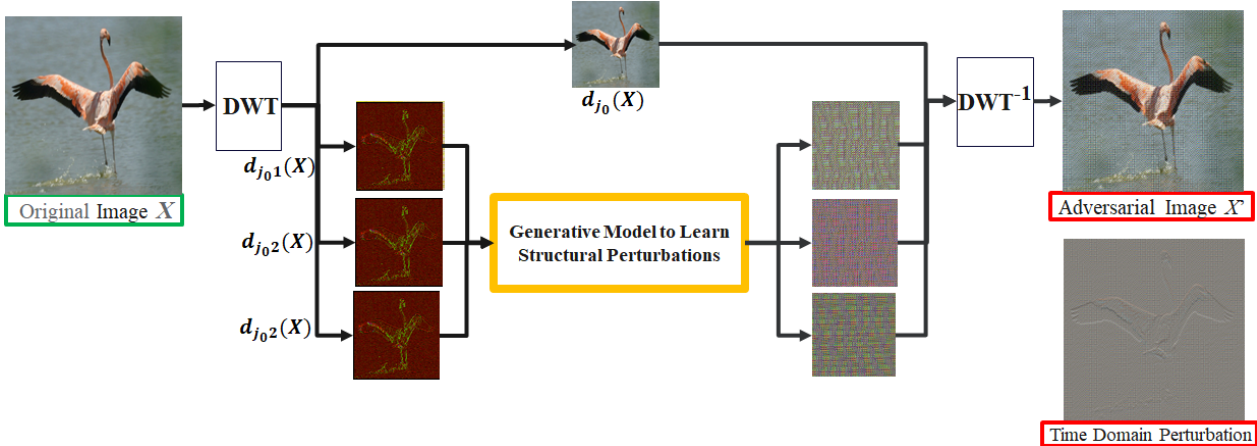


Figure 3. Overview of the proposed adversarial attack.

in Pytorch. Pretrained are from the TorchVision library and <https://github.com/thu-ml/Prior-Guided-RGF>.

4.1. Attack and defense comparison with generative-based models

To evaluate black-box attack transferability (no access to training data, nor the target model), we implemented adversarial attacks using Inception-v3 as a surrogate model. Testing models include ResNet-50 [13], VGG-16 [38]. To evaluate attack and defense, we use three state-of-the-art defense approaches: JPEG compression [11], Guided Denoiser [22], Randomization [47].

Table 1 shows fooling ratio in normal and defense performance for GAP [29], a modified GAP formulation with budget constraint (no wavelet integration) and WGAP. Overall, our model WGAP achieved best performance for scale level 1 and lowest for scale level 3. Interestingly, GAP showed best performance when using the testing networks ResNet-50, VGG-16 than the surrogate network Inception-v3. Best performance was obtained by WGAP, scale 1, across all budgets. Second-best performance was obtained by WGAP- $J_2(\epsilon_{k=1,2,3})$, and similar performance was obtained with GAP and WGAP- $J_3(\epsilon_{k=1,2,3})$. It is worth noting that, for a fixed budget, there is a decrease in fooling ratio performance from WGAP- $J_1(\epsilon_{k=1,2,3})$ (level 1) to WGAP- $J_3(\epsilon_{k=1,2,3})$ (level 3) and GAP($\epsilon_{k=1,2,3}$) (no wavelet). This suggests that defense approaches may not be tuned to overcome attacks from targeted frequency perturbations.

4.2. Attack and defense comparison for iterative (query-based) models

We further evaluate the transferability of the WGAP model by comparing performance with the Prior-guided Random Gradient-Free (P-RGF) [7]. We use the optimal

parameter λ^* and ResNet-152 as surrogate model [7]. The fooling ratio values for attack in normal models Inception-v3, ResNet-50 and VGG-16 are 91.1%, 99.6% and 97.7% respectively. Similarly, the number of iterations for the same models are: 649, 352 and 370. Fooling ratio for attacks in defense models JPEG Compression, Randomization and Guided Denoiser are 81.1%, 82.3% and 89.5% respectively. Whereas for number of iterations we obtained 2120, 1816 and 1784. As for the number of iterations, the optimized P-RGF_D achieved 99.1% in 649 iterations and the average time required to generate an adversarial attack was 15.15 seconds. While, P-RGF_D shows very high performance in attacks for both normal and defense models, the computationally complexity could be highly prohibitive to use in real time scenarios. Experimentally, we estimated an average time to produce an adversarial example, which was 209.21 seconds per image for P-RGF_D. The most similar performance in a defense network was in the Guided Denoiser² with a difference of 1.4%. Here, the P-RGF required 1816 iterations, approximately four times greater than the average number of iterations in normal models. It should be noted that the P-RGF requires access to the target model to iteratively estimate the gradient. While this may be useful in attacks where a model is available, there is a risk of generalizing and over fitting. Next, we provide an analysis to compare universal full black-box attacks and defense.

4.3. Transfer attacks and defense comparison

We compare model transferability from all approaches for black-box attack/defense and image error approximation in terms of the L2 norm. We test the state-of-the-art defense method Comdefend [17] against the generated images from the surrogate models: i) Inception-v3 for GAP and WGAP and ii) ResNet-152 for P-RGF [7]. This will

Method	Attacks in Normal Models			Attacks in Defense Models		
	Inception-v3	ResNet-50	VGG-16	JPEG Compression	Randomization	Guided Denoiser
GAP	69.4%	91.8%	90.3%	13.0%	14.1%	1.8 %
GAP(ϵ_1)	84.4%	89.5%	90.8%	10.7%	12.3%	13.4%
WGAP-J ₁ (ϵ_1)	91.1%	97.5%	98.5%	79.2%	73.5%	57.8%
WGAP-J ₂ (ϵ_1)	81.1%	96.5%	97.3%	69.1%	68.8%	33.9%
WGAP-J ₃ (ϵ_1)	34.2%	84.4%	88.7%	30.7%	30.3%	13.6%
GAP(ϵ_2)	92.6%	94.5%	97.1%	15.1%	17.5%	18.3%
WGAP-J ₁ (ϵ_2)	97.6%	98.9%	99.2%	96.2%	85.5%	86.9%
WGAP-J ₂ (ϵ_2)	85.4%	97.1%	99.3%	77.9%	76.0%	61.1%
WGAP-J ₃ (ϵ_2)	55.4%	89.1%	95.7%	51.1%	47.0%	22.8%
GAP(ϵ_3)	95.1%	98.6%	99.6%	23.3%	25.1%	29.8%
WGAP-J ₁ (ϵ_3)	99.4%	99.8%	99.7%	99.7%	93.6%	89.7%
WGAP-J ₂ (ϵ_3)	92.2%	98.0%	99.3%	87.8%	83.6%	68.9%
WGAP-J ₃ (ϵ_3)	56.3%	92.4%	95.7%	53.0%	44.5%	30.7%

Table 1. Fooling ratio performance comparison for attacks in normal and defense models. Inception-v3 is the surrogate model and the others are testing models. GAP is the method [29] with magnitude value of 10, WGAP for scales J1-J3 and budgets $\epsilon_1=0.05$, $\epsilon_2=0.1$, $\epsilon_3=0.25$.

	P-RGF _D (λ^*)	GAP	WGAP-J ₁ (ϵ_1)	WGAP-J ₂ (ϵ_1)	WGAP-J ₁ (ϵ_2)	WGAP-J ₂ (ϵ_2)
Comdefend	24.5%	28.3%	65.3%	77.5%	62.1%	69.5%
L2 Norm (%)	1.4 %	3.3%	4.2%	4.8 %	5.1%	5.4 %

Table 2. Performance comparison when the defense Comdefend method for fooling ratio and L2 Norm percentage.

provide an independent test on how general methods could be. Please note that for the iterative method, P-RGF we do not make any new query, we just used the generated image. Results are presented in Table 2. The first row shows the fooling ratio from all models (higher is better), second row shows the estimated L2 norm (lower is better). We note that P-RGF and GAP corresponds to the poorest performance when estimating fooling ratio: 24.5% and 28.3% respectively. However, the L2 norm values 1.4% and 3.3% for P-RGF and GAP are the lowest. For WGAP-based fooling ratio, the values for WGAP-J₁(ϵ_1) and WGAP-J₂(ϵ_1) were 65.3% and 77.5% respectively, while for WGAP-J₁(ϵ_2) and WGAP-J₂(ϵ_2) the fooling ratio values were 62.1% and 69.1% respectively. We note that while there was a significance increase in performance from budget $\epsilon_1=0.05$ to $\epsilon_2=0.1$, there was not a significant increase in L2 norm. For WGAP, we noticed that the L2 norm error was close to 5% even the budget was close to 10%. This may be because the network prioritizes perturbations with no major penalty to the budget. However, there may be significant qualitative visual differences between budgets. We note that the fooling ratio increases as wavelet coefficients go from details to approximations. This indicates that details (high) frequency perturbation patterns may be most meaningful when disrupting early convolutional layers from the network.

Figure 4 and Figure 5 depict example adversarial and residual images for each model (we omit other models due to space constraints). Column one in Figure 4, shows original images with corresponding class label. Column two and three corresponds to P-RGF [7], and GAP [29] respectively. Columns four and five corresponds to our proposed method with WGAP-J₁(ϵ_1) and WGAP-J₁(ϵ_2) with scale 1 and budget $\epsilon_1=0.05$, $\epsilon_2=0.1$.

Figures 4(b,c) and Figures 4(g,h) show an example where the defense network Comdefend, correctly classified the adversarial image. Figures 4(d,e) incorrectly classified the original image, with class name Thimble and Bucket. For Figure 4(l), while the defense network incorrectly classified the original image as oxygen mask, the prediction is semantically similar to the original category (gasmask). Figures 4(n,o) show the predictions from our method corresponding to Strainer and Zebra. We notice that the most semantics difference are in relation to the budget.

Images in Figures 5(a,f,k) show the original images. Images in Figures 5(b,g,l) show the residual for the P-RGF method. We can observe minimum perturbation across all images and without sign of a defined pattern across any image. Figures 5(c,h,m) show the result of the perturbation when GAP method was applied. A uniform pattern can be observed across the image. This is due to the outcome of

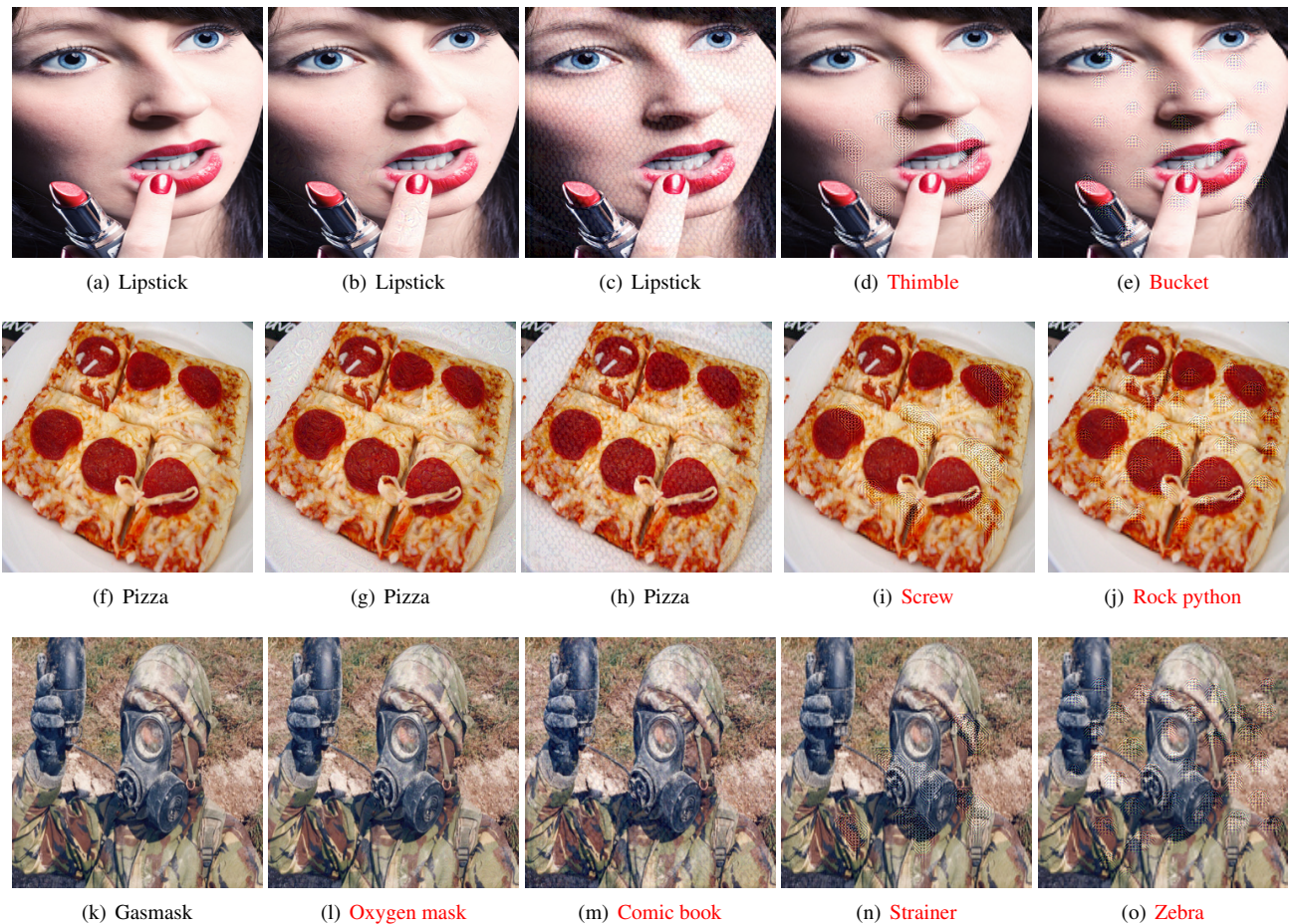


Figure 4. Adversarial examples from adversarial attack methods. First column ((a),(f),(k)) corresponds to the original image . Second column ((b),(g),(l)) corresponds to the adversarial example generated by the P-RGF method with optimal parameter λ^* . Third column ((c),(h),(m)) corresponds to the GAP method, a parameter value of 10 was set as proposed in the original method. Fourth ((d),(i),(n)) and fifth ((e),(j),(o)) columns corresponds to our proposed method $WGAP-J_1(\epsilon_1)$ and $WGAP-J_1(\epsilon_2)$, with budget $\epsilon_1 = 0.05$ and $\epsilon_1 = 0.1$ for L2 norm respectively.

the universal attack. Figures 5(d,i,n) and Figures 5(e,j,o) show the perturbations from our method at scale 1 and budgets 0.05 and 0.1, respectively. In contrast with the other two methods, we can observe that the perturbation pattern is heterogenous and non-uniformly distributed across the image. The perturbations is minimum at the background, either uniform (Figures 5(d,e) or Figures 5(i,j)) or heterogeneous (Figures 5(n,o)). Also, we note that the perturbations are consistently higher at the edges (as expected) and seems to increase for larger budget. Similarly, we observe some ‘texture-like’ patterns within the object of interest distributed across the foreground and backgrounds which seems to adapt according to the complexity of the image texture. This may indicate adaptive changes in the fine detail structure within the image according to the budget. For example, in Figure 5(d) there are 6 ‘texture-like’ patterns,

whereas in Figure 5(e) seems there are approximately 28 ‘texture-like’ patterns distributed in the foreground. Similar ‘texture-like’ patterns are found in the residuals relative to the other images. While this effect, will require more investigation, our experimental results may suggest that the frequency spectrum is affected differently depending on the scale, budget and object of interest.

5. Conclusions

We presented a new formulation for black-box attacks via time-scale (wavelets) analysis. Our approach performs adversarial attacks where there is no access to model nor dataset on which the target model has been trained. We make no assumptions about the image type or the target model and we provide extensive validation comparing our

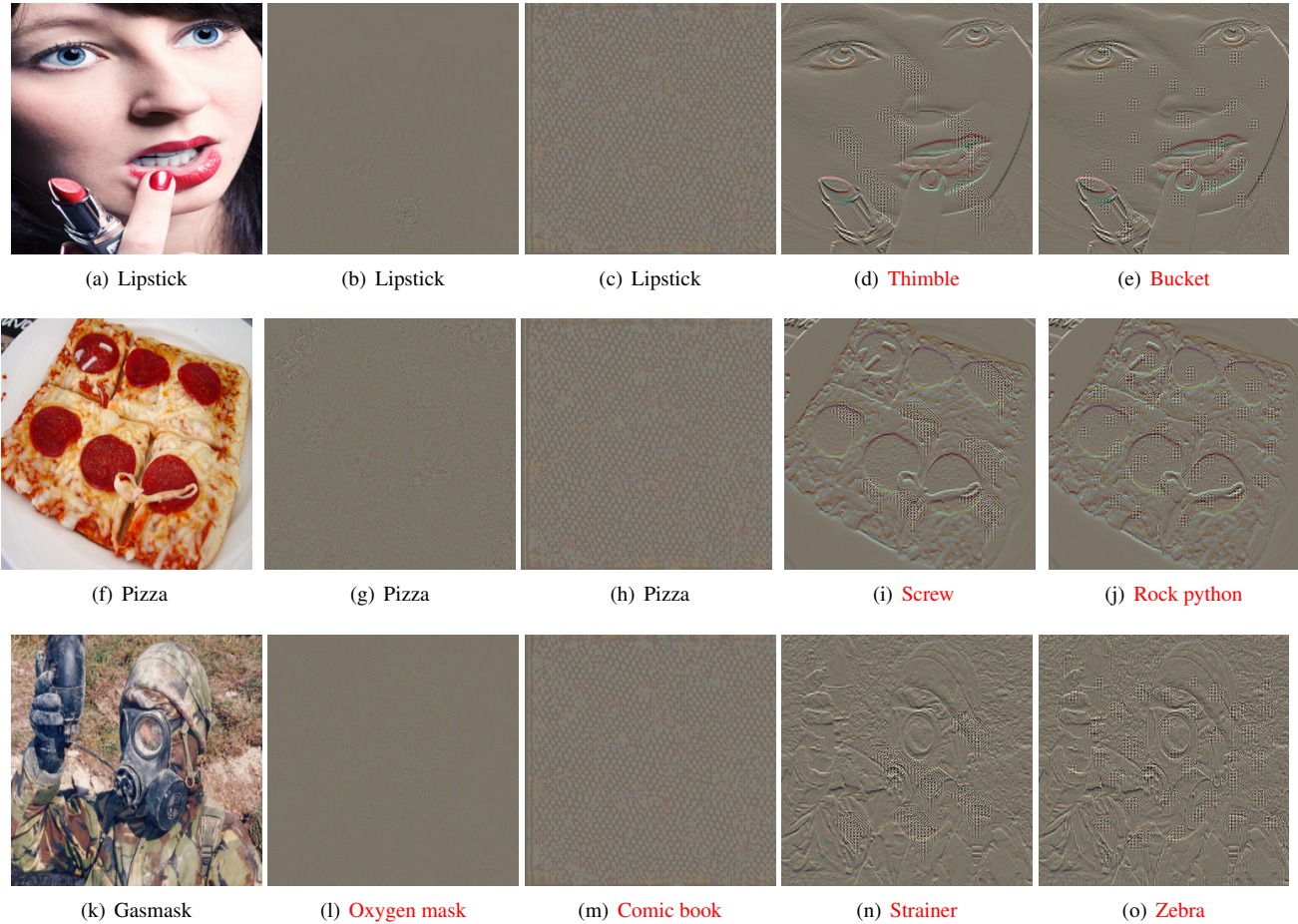


Figure 5. Residual images from adversarial attack methods. First column ((a),(f),(k)) corresponds to the original image . Second column ((b),(g),(l)) corresponds to the adversarial example generated by the P-RGF method with optimal parameter λ^* . Third column ((c),(h),(m)) corresponds to the GAP method. Fourth ((d),(i),(n)) and fifth ((e),(j),(o)) columns corresponds to our proposed method WGAP-J₁(ϵ_1) and WGAP-J₁(ϵ_2) , with budget $\epsilon_1 = 0.05$ and $\epsilon_1 = 0.1$ for L2 norm respectively.

approach with two state-of-the-art adversarial attacks methods and four state-of-the-art defense algorithms. Our results suggest that it is both feasible and effective to localize coherent spatial arrangements as a mechanism to disrupt CNN layer responses.

Our effort provides the first mathematical framework in terms of image analysis and signal processing for creating attacks to understand underlying vulnerability of convolution layers in neural networks. Even though time domain attacks are capable of effectively disrupting CNNs, it is difficult to interpret and systematically study the nature of the perturbations themselves. Moreover, by producing attacks from the perspective of wavelets, we seek to inspire research in academic community to look at decades of research in signal processing on wavelet transforms to study neural network properties and explore new architectures. This will in turn help us build up a general theory of how and why cer-

tain scales, orientations and frequency sub-bands affect neural networks. This will potentially lead to an understanding of CNN's vulnerability, providing the broader community with mathematical conditions to avoid unfavorable architectural choices.

To the best of our knowledge this is the first time that time-scale analysis has been used for adversarial attacks. The systematic analysis of the wavelet-based attacks will further provide a signal processing framework for understanding fundamental reasons for the brittleness in state-of-the-art DL models. The current research will be extended to provide the community with mathematical conditions to improve DL architectures and avoid choices that beget model fragility.

References

- [1] Arjun Nitin Bhagoji, Warren He, Bo Li, and Dawn Song. Practical Black-Box Attacks on Deep Neural Networks Using Efficient Query Mechanisms. In Vittorio Ferrari, Martial Hebert, Cristian Sminchisescu, and Yair Weiss, editors, *Computer Vision – ECCV 2018*, volume 11216, pages 158–174. Springer International Publishing, Cham, 2018. Series Title: Lecture Notes in Computer Science. **2**
- [2] Ali Borji. Pros and cons of GAN evaluation measures. *Computer Vision and Image Understanding*, 179:41–65, Feb. 2019. **1**
- [3] Thomas Brunner, Frederik Diehl, Michael Truong Le, and Alois Knoll. Guessing Smart: Biased Sampling for Efficient Black-Box Adversarial Attacks. pages 4958–4966, 2019. **1**
- [4] Nicholas Carlini, Anish Athalye, Nicolas Papernot, Wieland Brendel, Jonas Rauber, Dimitris Tsipras, Ian Goodfellow, Aleksander Madry, and Alexey Kurakin. On Evaluating Adversarial Robustness. *arXiv:1902.06705 [cs, stat]*, Feb. 2019. arXiv: 1902.06705. **1**
- [5] Nicholas Carlini and David Wagner. Adversarial Examples Are Not Easily Detected: Bypassing Ten Detection Methods. In *Proceedings of the 10th ACM Workshop on Artificial Intelligence and Security, AISec ’17*, pages 3–14, Dallas, Texas, USA, Nov. 2017. Association for Computing Machinery. **2**
- [6] Pin-Yu Chen, Huan Zhang, Yash Sharma, Jinfeng Yi, and Cho-Jui Hsieh. ZOO: Zeroth Order Optimization based Black-box Attacks to Deep Neural Networks without Training Substitute Models. *Proceedings of the 10th ACM Workshop on Artificial Intelligence and Security - AISec ’17*, pages 15–26, 2017. arXiv: 1708.03999. **1, 2**
- [7] Shuyu Cheng, Yinpeng Dong, Tianyu Pang, Hang Su, and Jun Zhu. Improving Black-box Adversarial Attacks with a Transfer-based Prior. *arXiv:1906.06919 [cs, stat]*, Oct. 2019. arXiv: 1906.06919. **2, 4, 5, 6**
- [8] I. Daubechies. The wavelet transform, time-frequency localization and signal analysis. *IEEE Transactions on Information Theory*, 36(5):961–1005, Sept. 1990. Conference Name: IEEE Transactions on Information Theory. **2, 4**
- [9] Kathrin Grosse, Praveen Manoharan, Nicolas Papernot, Michael Backes, and Patrick McDaniel. On the (Statistical) Detection of Adversarial Examples. *arXiv:1702.06280 [cs, stat]*, Oct. 2017. arXiv: 1702.06280. **2**
- [10] Chuan Guo, Jared S. Frank, and Kilian Q. Weinberger. Low Frequency Adversarial Perturbation. *arXiv:1809.08758 [cs]*, July 2019. arXiv: 1809.08758. **2**
- [11] Chuan Guo, Mayank Rana, Moustapha Cisse, and Laurens van der Maaten. Countering Adversarial Images using Input Transformations. *arXiv:1711.00117 [cs]*, Jan. 2018. arXiv: 1711.00117. **5**
- [12] Jamie Hayes and George Danezis. Learning Universal Adversarial Perturbations with Generative Models. *arXiv:1708.05207 [cs, stat]*, Jan. 2018. arXiv: 1708.05207. **2**
- [13] Kaiming He, Xiangyu Zhang, Shaoqing Ren, and Jian Sun. Deep Residual Learning for Image Recognition. pages 770–778, 2016. **5**
- [14] Christopher Heil and Gitta Kutyniok. The Homogeneous Approximation Property for wavelet frames. *Journal of Approximation Theory*, 147(1):28–46, July 2007. **2**
- [15] Gao Huang, Zhuang Liu, Laurens van der Maaten, and Kilian Q. Weinberger. Densely Connected Convolutional Networks. *arXiv:1608.06993 [cs]*, Jan. 2018. arXiv: 1608.06993.
- [16] Andrew Ilyas, Logan Engstrom, and Aleksander Madry. Prior Convictions: Black-Box Adversarial Attacks with Bandits and Priors. *arXiv:1807.07978 [cs, stat]*, Mar. 2019. arXiv: 1807.07978. **1, 2**
- [17] Xiaojun Jia, Xingxing Wei, Xiaochun Cao, and Hassan Foroosh. ComDefend: An Efficient Image Compression Model to Defend Adversarial Examples. pages 6084–6092, 2019. **5**
- [18] Ameya Joshi, Amitangshu Mukherjee, Soumik Sarkar, and Chinmay Hegde. Semantic adversarial attacks: Parametric transformations that fool deep classifiers. In *Proceedings - 2019 International Conference on Computer Vision, ICCV 2019*, pages 4772–4782. Institute of Electrical and Electronics Engineers Inc., Oct. 2019. **2**
- [19] Saeed Reza Kheradpisheh, Masoud Ghodrati, Mohammad Ganjtabesh, and Timothée Masquelier. Deep Networks Can Resemble Human Feed-forward Vision in Invariant Object Recognition. *Scientific Reports*, 6, Sept. 2016. **1**
- [20] Xin Li and Fuxin Li. Adversarial Examples Detection in Deep Networks with Convolutional Filter Statistics. In *2017 IEEE International Conference on Computer Vision (ICCV)*, pages 5775–5783, Oct. 2017. ISSN: 2380-7504. **1**
- [21] Yingwei Li, Song Bai, Cihang Xie, Zhenyu Liao, Xiaohui Shen, and Alan L. Yuille. Regional Homogeneity: Towards Learning Transferable Universal Adversarial Perturbations Against Defenses. *arXiv:1904.00979 [cs]*, Apr. 2019. arXiv: 1904.00979. **2**
- [22] Fangzhou Liao, Ming Liang, Yinpeng Dong, Tianyu Pang, Xiaolin Hu, and Jun Zhu. Defense Against Adversarial Attacks Using High-Level Representation Guided Denoiser. pages 1778–1787, 2018. **5**
- [23] Stephane Mallat. A Wavelet Tour of Signal Processing : Stephane Mallat : 9780123743701. **2**
- [24] Stéphane Mallat. Understanding Deep Convolutional Networks. *Philosophical Transactions of the Royal Society A: Mathematical, Physical and Engineering Sciences*, 374(2065):20150203, Apr. 2016. arXiv: 1601.04920. **2**
- [25] Seyed-Mohsen Moosavi-Dezfooli, Alhussein Fawzi, Omar Fawzi, and Pascal Frossard. Universal adversarial perturbations. *arXiv:1610.08401 [cs, stat]*, Mar. 2017. arXiv: 1610.08401. **1**
- [26] Konda Reddy Mopuri, Aditya Ganeshan, and R. Venkatesh Babu. Generalizable Data-Free Objective for Crafting Universal Adversarial Perturbations. *IEEE Transactions on Pattern Analysis and Machine Intelligence*, 41(10):2452–2465, Oct. 2019. Conference Name: IEEE Transactions on Pattern Analysis and Machine Intelligence. **2**
- [27] Konda Reddy Mopuri, Utsav Garg, and R. Venkatesh Babu. Fast Feature Fool: A data independent approach to universal adversarial perturbations. *arXiv:1707.05572 [cs]*, July 2017. arXiv: 1707.05572. **2**

- [28] Nikolaos Pitropakis, Emmanouil Panaousis, Thanassis Giannetsos, Eleftherios Anastasiadis, and George Loukas. A taxonomy and survey of attacks against machine learning. *Computer Science Review*, 34:100199, Nov. 2019. [2](#)
- [29] Omid Poursaeed, Isay Katsman, Bicheng Gao, and Serge Belongie. Generative Adversarial Perturbations. *arXiv:1712.02328 [cs, stat]*, July 2018. *arXiv: 1712.02328*. [2](#), [4](#), [5](#), [6](#)
- [30] Aaditya Prakash, Nick Moran, Solomon Garber, Antonella DiLillo, and James Storer. Deflecting Adversarial Attacks With Pixel Deflection. pages 8571–8580, 2018. [2](#)
- [31] Olga Russakovsky, Jia Deng, Hao Su, Jonathan Krause, Sanjeev Satheesh, Sean Ma, Zhiheng Huang, Andrej Karpathy, Aditya Khosla, Michael Bernstein, Alexander C. Berg, and Li Fei-Fei. ImageNet Large Scale Visual Recognition Challenge. *arXiv:1409.0575 [cs]*, Jan. 2015. *arXiv: 1409.0575*. [4](#)
- [32] Ahmed Salem, Yang Zhang, Mathias Humbert, Pascal Berrang, Mario Fritz, and Michael Backes. ML-Leaks: Model and Data Independent Membership Inference Attacks and Defenses on Machine Learning Models. *arXiv:1806.01246 [cs]*, Dec. 2018. *arXiv: 1806.01246*. [1](#)
- [33] Pouya Samangouei, Maya Kabkab, and Rama Chellappa. Defense-GAN: Protecting Classifiers Against Adversarial Attacks Using Generative Models. *arXiv:1805.06605 [cs, stat]*, May 2018. *arXiv: 1805.06605*. [1](#)
- [34] Sayantan Sarkar, Ankan Bansal, Upal Mahbub, and Rama Chellappa. UPSET and ANGRI : Breaking High Performance Image Classifiers. *arXiv:1707.01159 [cs]*, July 2017. *arXiv: 1707.01159*. [2](#)
- [35] Ali Shafahi, Mahyar Najibi, Mohammad Amin Ghiasi, Zheng Xu, John Dickerson, Christoph Studer, Larry S Davis, Gavin Taylor, and Tom Goldstein. Adversarial training for free! In H. Wallach, H. Larochelle, A. Beygelzimer, F. d\textquotesingle Alch -Buc, E. Fox, and R. Garnett, editors, *Advances in Neural Information Processing Systems 32*, pages 3358–3369. Curran Associates, Inc., 2019. [2](#)
- [36] Ali Shafahi, Mahyar Najibi, Zheng Xu, John Dickerson, Larry S. Davis, and Tom Goldstein. Universal Adversarial Training. *arXiv:1811.11304 [cs]*, Nov. 2019. *arXiv: 1811.11304*. [2](#)
- [37] Mahmood Sharif, Sruti Bhagavatula, Lujo Bauer, and Michael K. Reiter. A General Framework for Adversarial Examples with Objectives. *ACM Transactions on Privacy and Security*, 22(3):1–30, July 2019. [2](#)
- [38] Karen Simonyan and Andrew Zisserman. Very Deep Convolutional Networks for Large-Scale Image Recognition. *arXiv:1409.1556 [cs]*, Apr. 2015. *arXiv: 1409.1556*. [5](#)
- [39] David Stutz, Matthias Hein, and Bernt Schiele. Disentangling Adversarial Robustness and Generalization. pages 6976–6987, 2019. [2](#)
- [40] Jiawei Su, Danilo Vasconcellos Vargas, and Kouichi Sakurai. One Pixel Attack for Fooling Deep Neural Networks. *IEEE Transactions on Evolutionary Computation*, 23(5):828–841, Oct. 2019. Conference Name: IEEE Transactions on Evolutionary Computation. [2](#)
- [41] Dimitris Tsipras, Shibani Santurkar, Logan Engstrom, Alexander Turner, and Aleksander Madry. Robustness May Be at Odds with Accuracy. *arXiv:1805.12152 [cs, stat]*, Sept. 2019. *arXiv: 1805.12152* version: 2. [1](#)
- [42] Danilo Vasconcellos Vargas and Shashank Kotyan. Robustness Assessment for Adversarial Machine Learning: Problems, Solutions and a Survey of Current Neural Networks and Defenses. *arXiv:1906.06026 [cs, stat]*, Nov. 2019. *arXiv: 1906.06026*. [2](#)
- [43] B. S. Vivek, Konda Reddy Mopuri, and R. Venkatesh Babu. Gray-Box Adversarial Training. In Vittorio Ferrari, Martial Hebert, Cristian Sminchisescu, and Yair Weiss, editors, *Computer Vision – ECCV 2018*, volume 11219, pages 213–228. Springer International Publishing, Cham, 2018. Series Title: Lecture Notes in Computer Science. [2](#)
- [44] Eric Wong and J Zico Kolter. Provable Defenses against Adversarial Examples via the Convex Outer Adversarial Polytope. page 10. [1](#)
- [45] Chaowei Xiao, Ruizhi Deng, Bo Li, Taesung Lee, Benjamin Edwards, Jinfeng Yi, Dawn Song, Mingyan Liu, and Ian Molloy. AdvIT: Adversarial frames identifier based on temporal consistency in videos. In *Proceedings - 2019 International Conference on Computer Vision, ICCV 2019*, pages 3967–3976. Institute of Electrical and Electronics Engineers Inc., Oct. 2019. [2](#)
- [46] Chaowei Xiao, Ruizhi Deng, Bo Li, Fisher Yu, Mingyan Liu, and Dawn Song. Characterizing Adversarial Examples Based on Spatial Consistency Information for Semantic Segmentation. In Vittorio Ferrari, Martial Hebert, Cristian Sminchisescu, and Yair Weiss, editors, *Computer Vision – ECCV 2018*, volume 11214, pages 220–237. Springer International Publishing, Cham, 2018. Series Title: Lecture Notes in Computer Science. [2](#)
- [47] Cihang Xie, Jianyu Wang, Zhishuai Zhang, Zhou Ren, and Alan Yuille. Mitigating Adversarial Effects Through Randomization. *arXiv:1711.01991 [cs]*, Feb. 2018. *arXiv: 1711.01991*. [5](#)
- [48] Cihang Xie, Jianyu Wang, Zhishuai Zhang, Yuyin Zhou, Lingxi Xie, and Alan Yuille. Adversarial Examples for Semantic Segmentation and Object Detection. In *2017 IEEE International Conference on Computer Vision (ICCV)*, pages 1378–1387, Oct. 2017. ISSN: 2380-7504. [2](#)
- [49] Matthew D. Zeiler and Rob Fergus. Visualizing and Understanding Convolutional Networks. In David Fleet, Tomas Pajdla, Bernt Schiele, and Tinne Tuytelaars, editors, *Computer Vision – ECCV 2014*, Lecture Notes in Computer Science, pages 818–833, Cham, 2014. Springer International Publishing. [1](#)